Water Splits Epitaxial Graphene and Intercalates

Xiaofeng Feng,[†,‡] Sabine Maier,[†,§] and Miquel Salmeron*[†,‡]

[†]Materials Sciences Division, Lawrence Berkeley National Laboratory, Berkeley, California 94720, United States
[‡]Department of Materials Science and Engineering, University of California, Berkeley, California 94720, United States

Ⓢ *Supporting Information*

ABSTRACT: The adsorption and reactions of small molecules, such as water and oxygen, with graphene films is an area of active research, as graphene may hold the key to unique applications in electronics, batteries, and other technologies. Since the graphene films produced so far are typically polycrystalline, with point and line defects that can strongly affect gas adsorption, there is a need to understand their reactivity with environmentally abundant molecules that can adsorb and alter their properties. Here we report a study of the adsorption and reactions of water, oxygen, hydrogen, and ammonia on epitaxial graphene grown on Ru and Cu substrates using scanning tunneling microscopy (STM). We found that on Ru(0001) graphene line defects are extremely fragile toward chemical attack by water, which splits the graphene film into numerous fragments at temperatures as low as 90 K, followed by water intercalation under the graphene. On Cu(111) water can also split graphene but far less effectively, indicating that the chemical nature of the substrate strongly affects the reactivity of the C−C bonds in epitaxial graphene. Interestingly, no such effects were observed with other molecules, including oxygen, hydrogen, and ammonia also studied here.
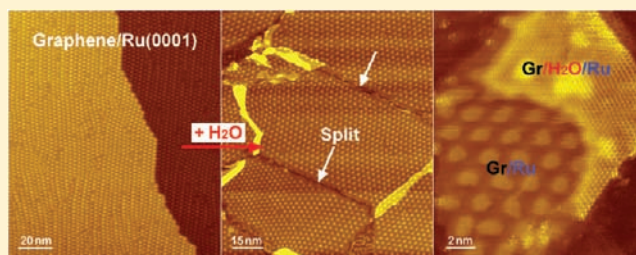
■ INTRODUCTION

Graphene, a single layer of carbon atoms bonded in a hexagonal lattice, has attracted intense scientific interest due to its unique two-dimensional structure and remarkable electronic properties, which make it a promising material for large-scale applications in nanoelectronics.[1,2] Graphite and graphene films are also important in battery technologies, as they are used as intercalation hosts for Li ions.[3] For some of these applications, controllable synthesis of large-area and high-quality graphene is required. Epitaxial growth of graphene on metal substrates such as Ru,[4,5] Ir,[6] and Cu[7,8] has been demonstrated to be a rational route for producing macroscopic graphene films. However, the as-produced graphene films are typically polycrystalline,[9] with point defects (such as vacancies and nonhexagonal rings) and line defects (dislocations and grain boundaries)[10] that can markedly affect their properties, such as mechanical strength,[9] electrical transport,[11] and chemical reactivity.[12] It is therefore of great importance to study the impact of these defects on the chemical and structural properties of epitaxial graphene.

Another important concern is that graphene-based devices are normally operated in ambient environments, where the gas molecules (such as H_2O, O_2) may react with the graphene and degrade their performance and reliability.[1,13−15] For example, exposure of annealed graphene films to water vapor or ammonia leads to their p-type or n-type doping,[1] while the controlled adsorption of water molecules can be used to tune the bandgap in graphene.[13] Similarly, oxygen can also produce hole-doping in deformed graphene.[14] The gas molecules adsorbed on graphene can act as donors or acceptors and induce changes in the electrical conductivity, giving rise to such applications as gas sensors with high sensitivity.[15] The influence of gas adsorption becomes more severe when graphene contains defects due to their enhanced reactivity.[16,17] For example, water molecules can dissociate over defective sites in graphene, forming C−H and C−OH bonds, which has been demonstrated by both theoretical calculations[18] and vibrational spectroscopy.[19] Therefore, elucidating the impact of defects toward gas adsorption and reactions is crucial for making reliable graphene-based devices that are operated at ambient conditions.

In this article, we report a study, using scanning tunneling microscopy (STM), of water adsorption and reactions on epitaxial graphene on Ru and Cu substrates. These two metal substrates have been intensely explored for epitaxial graphene because of their potential for producing macroscopic graphene films.[5,7] We found that on Ru(0001) water splits the epitaxial graphene along line defects into numerous fragments at temperatures as low as 90 K, followed by water intercalation under the graphene. On Cu(111) however, the water-induced splitting of graphene is far less effective, indicating that the substrate plays a key role in modifying the chemical properties of epitaxial graphene. Our findings provide relevant and novel information on the reactivity of defects in graphene, which should be of great interest for both fundamental science and technological applications.
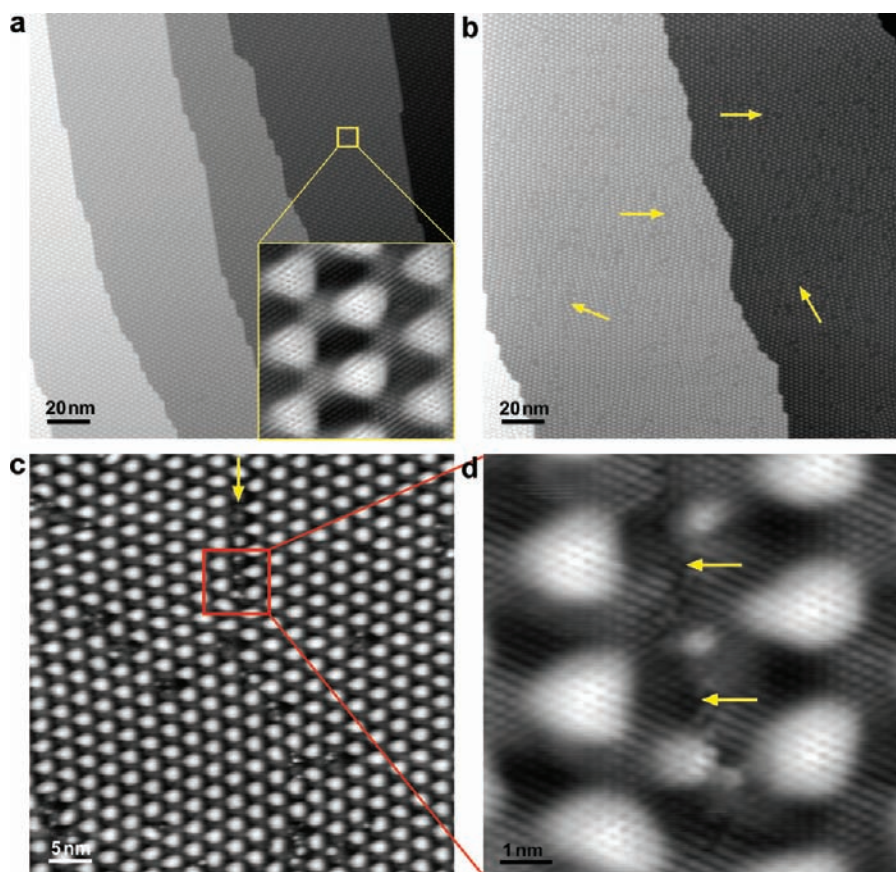
Figure 1. STM images of the as-grown graphene film on Ru(0001). (a) An overview of the graphene film, showing a Moiré pattern with a periodicity of around 3 nm. The atomically resolved superstructure is shown in the inset. (b) The quality of the graphene is not homogeneous over the surface, some areas containing numerous line defects, as indicated by the arrows. (c) Expanded view of an edge dislocation in graphene, as indicated by the arrow. (d) Close-up image of the area in the square in (c), showing the discontinuity of the graphene lattice, where dangling and stretched bonds are expected to occur. Imaging parameters: sample bias voltage V_s = 27 mV, tunneling current I_t = 12 pA (a); V_s = 150 mV, I_t = 15 pA (b); V_s = 15 mV, I_t = 0.29 nA (c,d).

■ EXPERIMENTAL SECTION

The experiments were performed using a home-built, low-temperature ultrahigh vacuum (UHV) STM at a base pressure below 3×10^{-11} Torr.[20] The Ru(0001) surface was cleaned first by Ar ion sputtering at 1 kV, followed by annealing and cooling cycles between 770 and 1770 K in a partial oxygen atmosphere to remove carbon impurities from the surface. The remaining oxygen on the surface was removed by annealing the sample to 1670 K in UHV. The cleanness of the surface was confirmed by Auger electron spectroscopy and STM. Epitaxial graphene on Ru was prepared by exposing the Ru sample to ethylene at 1230 K (2×10^{-7} Torr, 2 min). Epitaxial graphene on Cu(111) was prepared through exposure to ethylene at 1273 K (4×10^{-4} Torr, 15 min). The samples were then slowly cooled down and transferred to the STM body in a connected UHV chamber. Water (Sigma Aldrich, deuterium depleted, 99.99995%) was purified by freeze–pump–thaw cycles and dosed through a leak valve and a dosing tube pointing toward the sample at a defined sample temperature. After water exposure, the sample could be annealed to higher temperatures to enhance the mobility and reactivity. All STM images presented in this paper were acquired at 77 K.

■ RESULTS AND DISCUSSION

Figure 1a shows an STM image of the graphene film grown on the Ru(0001) substrate. A hexagonal lattice with a periodicity of about 3 nm is observed, which is a Moiré pattern due to the lattice mismatch between the graphene and Ru substrate.[4] The expanded STM image in the inset of Figure 1a shows the atomically resolved superstructure, which corresponds to (12 × 12) graphene unit cells sitting on (11 × 11) Ru unit cells.[4] Nevertheless, it should be noticed that a C(25 × 25)−Ru(23 × 23) superstructure has also been suggested.[21] The observed corrugation originates primarily from a geometric buckling of the graphene film,[22] which interacts strongly with the underlying Ru substrate. The quality of the graphene film is not homogeneous over the entire surface: some areas are almost defect-free (Figure 1a), while others contain line defects,[10] mainly dislocations and grain boundaries (Figures 1b and S1, Supporting Information (SI)). Figure 1c is an image of an edge dislocation, where an additional period of the Moiré pattern is inserted at the location indicated by an arrow. The atomic-scale details in Figure 1d reveal the discontinuity of the graphene lattice at the defect line, suggesting that broken and stretched C−C bonds occur there. The graphene domains across the line defects often show different orientations in the Moiré patterns (see Figure S1 (SI)), indicating their different lattice orientations relative to the Ru substrate.

The graphene-covered surface was exposed to submonolayer amounts of water (2×10^{-10} Torr, ~1 min) at 77 K. The adsorbed water formed clusters, as shown in Figure 2a, indicative of poor wetting. These clusters, visible as bright clumps around 1 to 2 nm high, were easily scraped away by the STM tip while imaging at low tunneling resistance (Figure S2 (SI)).[23] Imaging conditions with a negative sample bias voltage
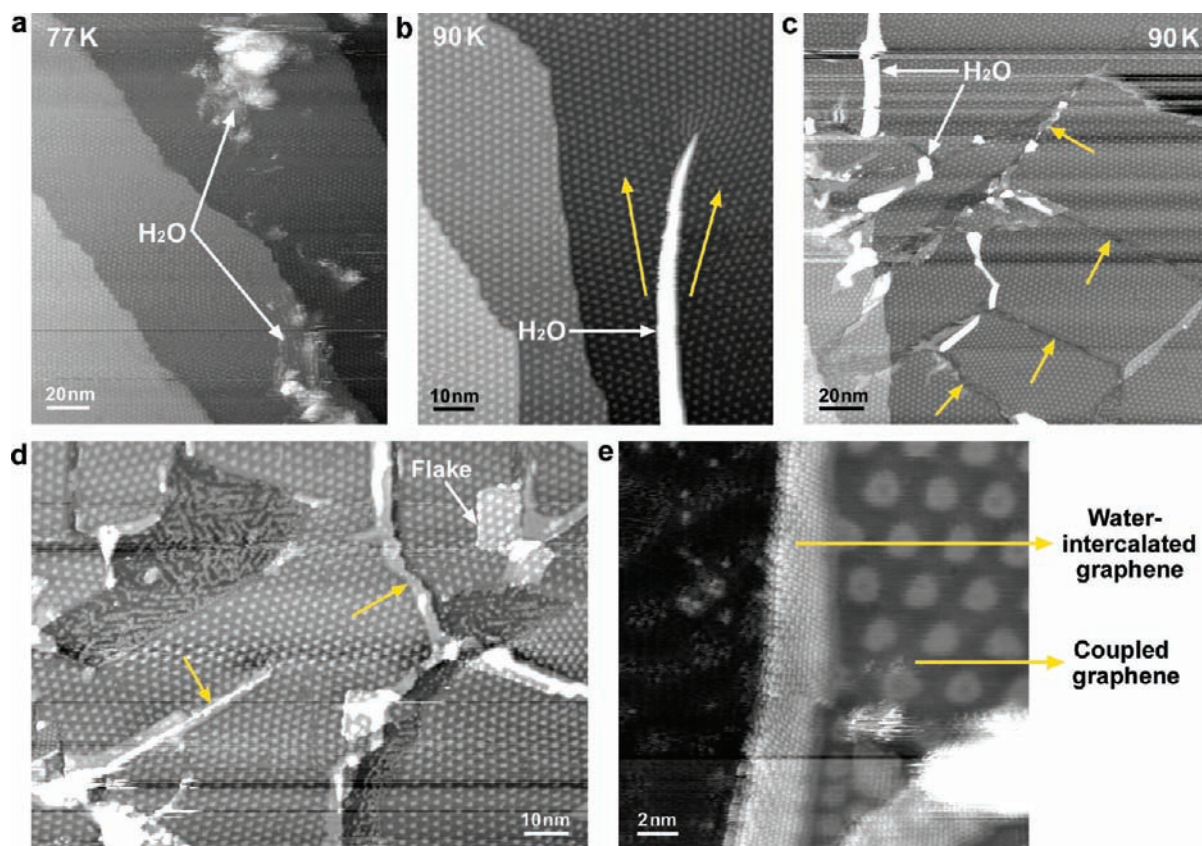
Figure 2. STM images of the graphene surface after water exposure. (a) Clusters are formed on top of the graphene surface after water exposure at 77 K. (b) After annealing to 90 K for 5 min, water stripes are observed decorating some defect lines. The Moiré patterns on each side show different orientations (as indicated by the arrows), indicating a dislocation there. (c) Graphene splits into fragments along line defects, opening gaps between them, as indicated by arrows. The bright stripes are attributed to water. (d) Graphene flakes detached from the substrate moved on top of the first overlayer. Exposed areas of Ru substrate decorated with water stripes are visible. Decoupled graphene (no Moiré pattern) due to water intercalation is observed along the edges of the split fragments, as indicated by the yellow arrows. (e) Expanded view image showing the atomic-scale structure of water intercalated graphene at the edge of a fragment. Imaging parameters: $V_s = -1.5$ V, $I_t = 4$ pA (a–d); $V_s = -16$ mV, $I_t = 0.5$ nA (e).

($|V_s| \geq 1.5$ V) and a low tunneling current (~5 pA), however, were found to give stable imaging (see the discussion in Figure S2 (SI)).[23] STM images acquired in different areas indicate that water is distributed inhomogenously, accumulating preferentially in defective areas.

Annealing the sample to 90 K for 5 min produced notable changes, as shown in Figure 2b–d. Water stripes are observed decorating some of the dislocation lines (Figure 2b). In many areas, the graphene film appears split into fragments separated by gaps (Figure 2c). The different orientations of the Moiré pattern in the fragments on each side of the gaps indicate that an edge dislocation or grain boundary was previously there. In addition to the splitting, graphene fragments were found detached and displaced away from the Ru substrate, forming flakes on top of other graphene areas, as shown in Figure 2d. The facile displacement of the flakes is indicative of a weak interaction with the graphene substrate, a topic of interest that has been treated theoretically.[24] It is clear from our results that even the small forces from tip–sample interaction or thermal agitation are capable of initiating the displacement. The displaced flakes show a Moiré pattern almost identical to that of the first graphene layer underneath (Figure S3 (SI)), indicating that the corrugation and orientation of the second graphene layer is similar to that of the first layer.[25] In addition, stripe-like water structures are observed on the exposed areas of the Ru substrate.

The detachment of graphene fragments is attributed to the intercalation of water that weakens the interaction of C with the Ru substrate. Intercalation is facilitated by the gaps opened by the splitting of the graphene at line defects. It propagates from the edges to the interior, as indicated in Figure 2d. The intercalated water decouples the graphene from the Ru substrate, causing the loss of the Moiré pattern, as shown in Figure 2e. Similar effects have been observed with other chemical species like oxygen.[26,27] Intercalation of water has also been observed between graphene and mica under humid environments,[28] indicating that water intercalated between graphene and a hydrophilic substrate (such as mica and Ru) is more energetically favorable. The structure of the intercalated water is of great interest but unfortunately is not revealed by the STM images, which show mostly a superposition of the atomic structure of the graphene and the intercalated layer. Confinement due to the intercalation might force different molecular orientations and hydrogen bonding geometries, as predicted theoretically for water confined between graphene sheets,[29] which may change the activation barrier for reactions, such as the dissociation of water.[30] This is a very interesting topic that deserves further investigation.

The process of graphene fragmentation, flake displacement, and water intercalation amplifies as more water is added to the surface at higher temperatures. Figure 3 shows STM images acquired after another submonolayer water exposure (2×10^{-10}
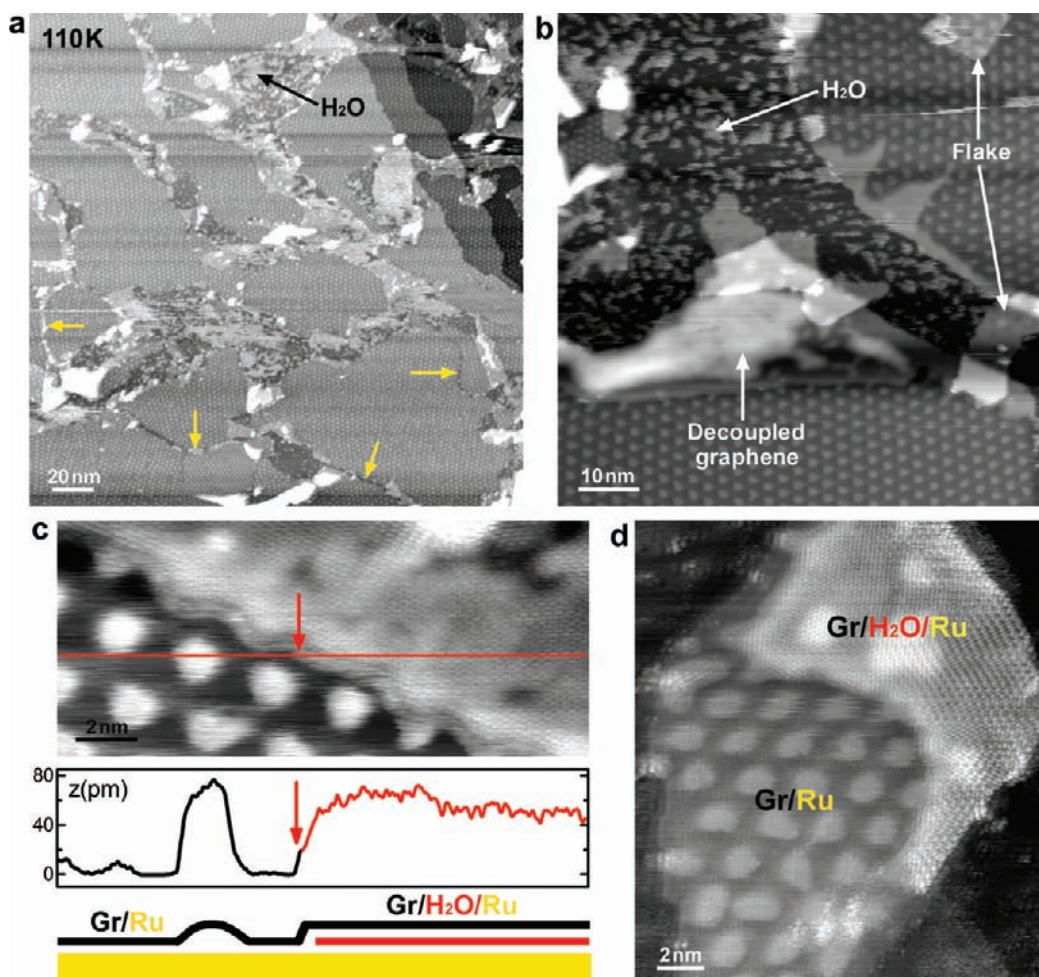
Figure 3. Additional water exposure at 110 K results in more graphene spitting and displacement. (a) STM image showing graphene splitting and flake detachment after an additional submonolayer amount of water was deposited at 110 K. More cracks are opened along line defects (as indicated by yellow arrows), and water adsorbs on exposed areas of the Ru substrate. (b) A close-up of the surface showing water on exposed Ru areas and decoupled graphene (no Moiré pattern) due to water intercalation underneath. (c,d) Atomically resolved images of graphene fragments partially intercalated with water, which decouples it from the Ru substrate (showing no Moiré pattern). Atomic structure of the graphene in the intercalated part is resolved. The uneven distribution of water underneath is responsible for the variations in contrast. A height profile following the red line is shown in (c) along with a schematic illustration below. Imaging parameters: $V_s = -1.5$ V, $I_t = 5$ pA (a,b); $V_s = -16$ mV, $I = 0.2$ nA (c); $V_s = -16$ mV, $I_t = 0.5$ nA (d).

Torr, ~1 min) at 110 K. More gaps are opened along line defects, as indicated by yellow arrows in Figure 3a, and more water is observed on the exposed Ru substrates. Meanwhile, the extent of water intercalation under the graphene has also increased, as shown in Figure 3b. Some of the intercalated graphene regions are relatively smooth, as shown in Figure 3c, and the height profile along the red line shows that the apparent height of the intercalated area is about 0.6−0.8 Å. In other intercalated regions, the surface topography is uneven with apparent heights varying from 1 Å to 5 Å (Figure 3d). These observations indicate that the spatial distribution and thickness of the water layer under the graphene is not uniform.[28]

After annealing to 200 K for 30 min, the water adsorbed on the exposed Ru substrate has completely dissociated forming a (2×1) structure (the inset of Figure 4a), which is known to be formed by adsorbed oxygen atoms.[31] Many more fragments of the initial graphene film have been split and displaced to other areas (about 50% in Figure 4a). Because the water-induced rupture of the graphene occurs at line defects, the resulting graphene flakes are defect-free. It is important to point out that

similar water exposure and annealing experiments on graphene areas with very few defects did not result in the splitting of graphene (see Figure S4 (SI)). The rupture of the strained C−C bonds at line defects should be facilitated by a catalytic interaction with the Ru substrate, as there are no reports of similar graphene splitting effects so far in the extensive work published about graphene on various substrates in humid environments. In contrast with other substrates, the epitaxial graphene on Ru(0001) is strongly corrugated by 1.5 Å, which may increase the stress and weaken the C−C bonds,[21,22] thus enhancing their reactivity, especially at the defects.[12] The dissociation of water at strained C−C bonds leading to their rupture is the key reaction that propagates and splits the graphene along line defects.[18,32−34] This process is reminiscent of the oxygen-driven unzipping of graphene[33,34] and carbon nanotubes,[35] while the difference is that here it occurs at a much lower temperature with water as the oxidant. The adsorption energy of water, ~0.40 eV on the Ru(0001) surface,[36] is comparable to the activation energy for oxygen intercalation between graphene and Ru (0.38 eV),[27] and thus
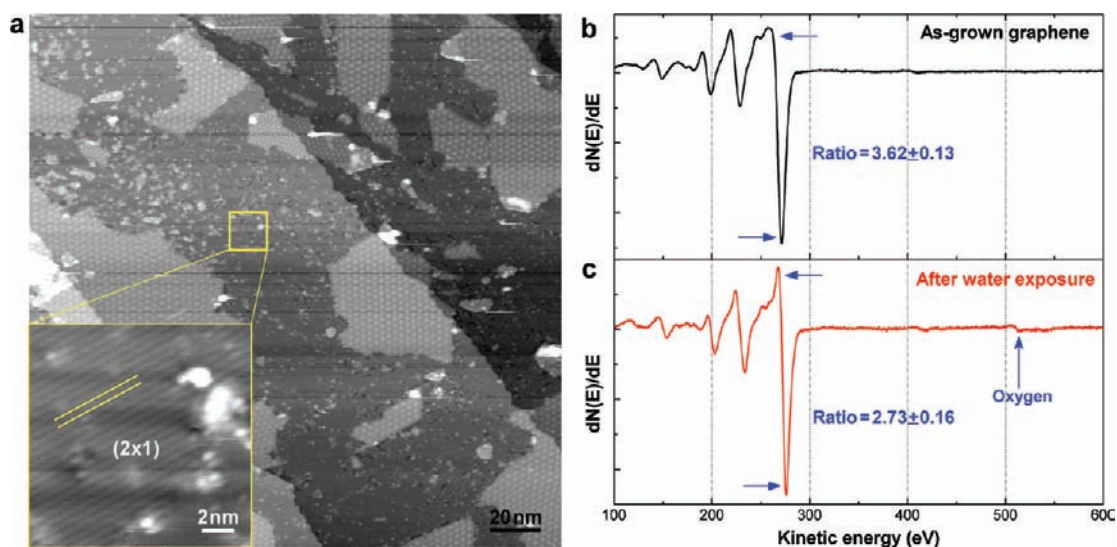
Figure 4. Thermal evolution of the water-exposed graphene surface. (a) Almost half of the graphene overlayer has been displaced after annealing to 200 K for 30 min. Water is dissociated, forming a (2×1) structure on the exposed Ru substrate, which are attributed to O atoms (inset). (b,c) Differential Auger spectra for the as-grown graphene (b) and water-exposed graphene (c), both acquired at 298 K. The peak ratio at 273 eV (lower half/upper half) decreased from 3.62 to 2.73, indicating a decrease in the carbon coverage. Meanwhile, the oxygen peak at ~512 eV became visible because of water dissociation.
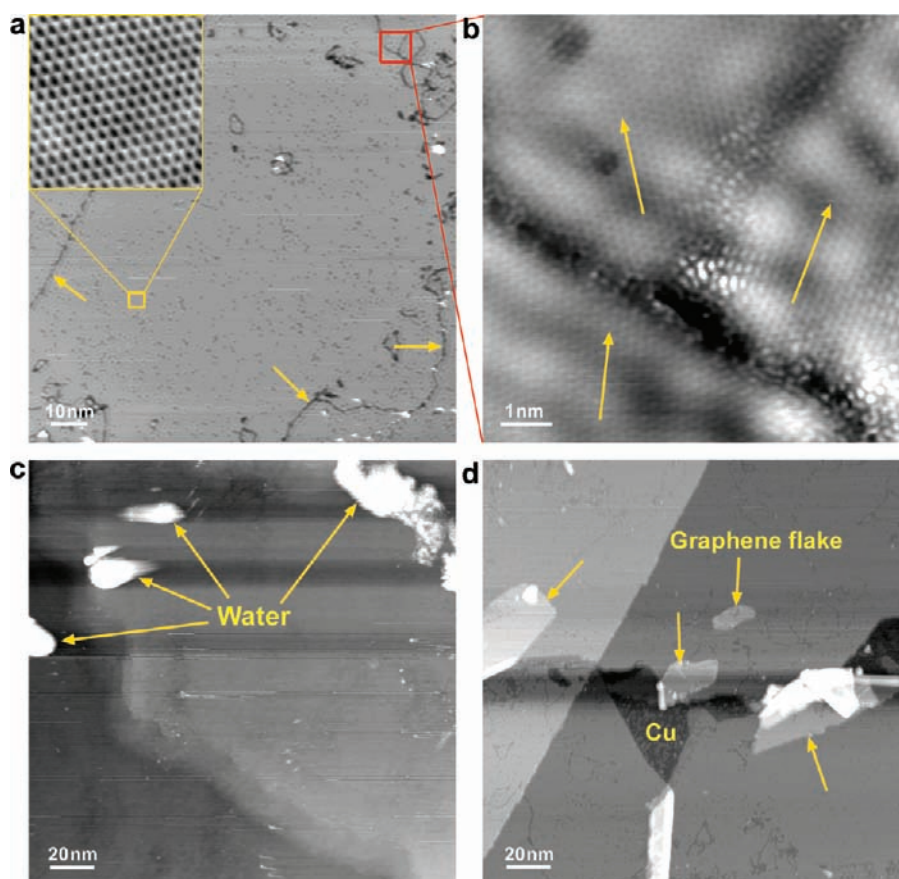
Figure 5. Water adsorption on graphene/Cu(111) surface. (a) An STM image of graphene on Cu(111), with an expanded view $(3.4 \times 3.4 \text{ nm}^2)$ showing the atomically resolved graphene lattice in the inset. The dark lines indicated by arrows mark the grain boundaries. (b) Expanded view of grain boundaries in the graphene (from the area in the red square in (a)), showing different lattice orientations (arrows) in each domain. (c) Water clusters on the graphene surface after submonolayer water exposure at 77 K. (d) After annealing to 150 K for 15 min, displaced graphene fragments were found occasionally, leaving the Cu substrate exposed. Imaging parameters: $V_s = 200$ mV, $I_t = 15$ pA (a); $V_s = 14$ mV, $I_t = 0.5$ nA (b); $V_s = -380$ mV, $I_t = 15$ pA (c,d).

should provide enough energy to facilitate the water intercalation.

Auger electron spectroscopy performed at room temperature shows an apparent decrease in the carbon coverage of the surface, as revealed by the decreased ratio between the intensities of the lower and upper half of the Ru 273 eV peak in the differential Auger spectrum.[4] In the as-grown graphene film, this ratio is 3.62 ± 0.13 (Figure 4b), corresponding to a high carbon coverage. The ratio decreased to 2.73 ± 0.16 after water exposure and annealing to 298 K (Figure 4c), indicating a reduced carbon coverage. This decrease is due to the displacement of flakes exposing bare Ru metal and forming double layers, so that the C peak is attenuated. Meanwhile, the oxygen peak at ∼512 eV becomes visible. Auger spectra of clean Ru(0001) and O(2 × 1)-covered Ru(0001) surfaces are shown in Figure S5 (SI).

To further elucidate the role of the Ru substrate in the splitting of graphene, comparative experiments were performed on epitaxial graphene on Cu(111) substrate, which was chosen because it interacts more weakly with graphene and does not dissociate water. Figure 5a shows an STM image of the graphene film on Cu(111) substrate, with an expanded image in the inset showing the atomically resolved structure. Dark lines are observed (indicated by arrows), which are due to grain boundaries.[8] An expanded view of grain boundaries is shown in Figure 5b, where the graphene lattice orientation is different in each domain. After water exposure at 77 K, water clusters are observed on the surface (Figure 5c), similar to the case of graphene on Ru. Subsequent annealing to temperatures below 150 K did not produce much difference. However, after annealing to 150 K for 15 min, some graphene fragments were found split from the film and displaced to other locations, as shown in Figure 5d. In contrast to the Ru case, the graphene splitting was found only occasionally on the Cu surface (about 1% area of the graphene film), indicating that the chemical nature of the substrate strongly affects the reactivity of the C−C bonds in epitaxial graphene.[37] In addition, we associate the occasional splitting of graphene observed on Cu substrate to the existence of more weakly interconnected domains, with a much higher density of dangling C−C bonds at the boundary, where water dissociation is facilitated.[18,19]

Finally, we also performed experiments with other molecules (O_2, H_2, NH_3), which, however, did not produce apparent changes to the graphene on Ru(0001) with gas partial pressures of up to 10^{-7} Torr and sample temperatures ranging from 77 to 298 K, indicating a much lower reactivity of these gases with the graphene.[26,27] The differences in reactivity between water and the other molecules on graphene is very intriguing[38] and calls for theoretical studies to fully understand the phenomenon.

CONCLUSIONS

In summary, we have shown that water efficiently splits epitaxial graphene on Ru(0001) at temperatures as low as 90 K, resulting in numerous graphene fragments. The graphene splitting initiates at line defects and is catalyzed by the underlying Ru substrate through weakening the C−C bonds at the defects. Water can also induce the splitting of graphene on Cu(111), but far less effectively. Our studies shed light on the impact of ambient gas adsorption on graphene, which can greatly affect the quality of graphene and thus be an important factor in graphene mass production and large-scale applications in electronics. From another perspective, the water-induced

splitting of graphene can eliminate grain boundaries and provide a method for tailoring graphene along line defects, with potential applications in the production of single-crystal nanosized graphene,[39] where defects could be introduced first using a variety of methods (seeded growth,[11] photo- and electron-beam lithography,[40] for example). The detachment of graphene films from metal substrates through water intercalation is also an attractive method worth exploring for graphene exfoliation, which possesses the merits of simplicity and reduced contamination. Intercalation is by itself an important step in batteries, where Li is stored between graphite sheets and other molecules can also insert. Our studies show a method for fundamental studies of these phenomena.

■ ASSOCIATED CONTENT

⑤ Supporting Information
Figures S1−S5, showing additional STM images of defects in the graphene; tip-induced scraping of water clusters at low tunneling resistance; atomically resolved images of graphene flakes; almost defect-free graphene areas after water exposure and annealing; STM images and Auger spectra of clean Ru(0001) and O(2 × 1)-covered Ru(0001) surfaces. This material is available free of charge via the Internet at http://pubs.acs.org.

■ AUTHOR INFORMATION

Corresponding Author
mbsalmeron@lbl.gov

Present Address
§Department of Physics, University of Erlangen-Nürnberg, 91058 Erlangen, Germany.

Notes
The authors declare no competing financial interest.

■ ACKNOWLEDGMENTS

■ REFERENCES

(1) Novoselov, K. S.; Geim, A. K.; Morozov, S. V.; Jiang, D.; Zhang, Y.; Dubonos, S. V.; Grigorieva, I. V.; Firsov, A. A. Science 2004, 306, 666−669.
(2) Geim, A. K.; Novoselov, K. S. Nat. Mater. 2007, 6, 183−191.
(3) Yoo, E.; Kim, J.; Hosono, E.; Zhou, H.; Kudo, T.; Honma, I. Nano Lett. 2008, 8, 2277−2282.
(4) Marchini, S.; Günther, S.; Wintterlin, J. Phys. Rev. B 2007, 76, 075429.
(5) Sutter, P. W.; Flege, J. I.; Sutter, E. A. Nat. Mater. 2008, 7, 406−411.
(6) Coraux, J.; N'Diaye, A. T.; Busse, C.; Michely, T. Nano Lett. 2008, 8, 565−570.
(7) Li, X.; Cai, W.; An, J.; Kim, S.; Nah, J.; Yang, D.; Piner, R.; Velamakanni, A.; Jung, I.; Tutuc, E.; Banerjee, S. K.; Colombo, L.; Ruoff, R. S. Science 2009, 324, 1312−1314.
(8) Gao, L.; Guest, J. R.; Guisinger, N. P. Nano Lett. 2010, 10, 3512−3516.
(9) Huang, P. Y.; Ruiz-Vargas, C. S.; van der Zande, A. M.; Whitney, W. S.; Levendorf, M. P.; Kevek, J. W.; Garg, S.; Alden, J. S.; Hustedt, C. J.; Zhu, Y.; Park, J.; McEuen, P. L.; Muller, D. A. Nature 2011, 469, 389−392.
(10) Banhart, F.; Kotakoski, J.; Krasheninnikov, A. V. ACS Nano 2011, 5, 26−41.

5667

dx.doi.org/10.1021/ja3003809 | J. Am. Chem. Soc. 2012, 134, 5662−5668

(11) Yu, Q.; Jauregui, L. A.; Wu, W.; Colby, R.; Tian, J.; Su, Z.; Cao, H.; Liu, Z.; Pandey, D.; Wei, D.; Chung, T. F.; Peng, P.; Guisinger, N. P.; Stach, E. A.; Bao, J.; Pei, S. S.; Chen, Y. P. *Nat. Mater.* **2011**, *10*, 443−449.

(12) Wang, B.; Puzyrev, Y.; Pantelides, S. T. *Carbon* **2011**, *49*, 3983−3988.

(13) Yavari, F.; Kritzinger, C.; Gaire, C.; Song, L.; Gullapalli, H.; Borca-Tasciuc, T.; Ajayan, P. M.; Koratkar, N. *Small* **2010**, *6*, 2535−2538.

(14) Ryu, S.; Liu, L.; Berciaud, S.; Yu, Y. J.; Liu, H.; Kim, P.; Flynn, G. W.; Brus, L. E. *Nano Lett.* **2010**, *10*, 4944−4951.

(15) Schedin, F.; Geim, A. K.; Morozov, S. V.; Hill, E. W.; Blake, P.; Katsnelson, M. I.; Novoselov, K. S. *Nat. Mater.* **2007**, *6*, 652−655.

(16) Jung, I.; Dikin, D.; Park, S.; Cai, W.; Mielke, S. L.; Ruoff, R. S. *J. Phys. Chem. C* **2008**, *112*, 20264−20268.

(17) Asai, M.; Ohba, T.; Iwanaga, T.; Kanoh, H.; Endo, M.; Campos-Delgado, J.; Terrones, M.; Nakai, K.; Kaneko, K. *J. Am. Chem. Soc.* **2011**, *133*, 14880−14883.

(18) Kostov, M. K.; Santiso, E. E.; George, A. M.; Gubbins, K. E.; Nardelli, M. B. *Phys. Rev. Lett.* **2005**, *95*, 136105.

(19) Politano, A.; Marino, A. R.; Formoso, V.; Chiarello, G. *AIP Adv.* **2011**, *1*, 042130.

(20) Shimizu, T. K.; Mugarza, A.; Cerda, J. I.; Heyde, M.; Qi, Y. B.; Schwarz, U. D.; Ogletree, D. F.; Salmeron, M. *J. Phys. Chem. C* **2008**, *112*, 7445−7454.

(21) Martoccia, D.; Willmott, P. R.; Brugger, T.; Björck, M.; Günther, S.; Schlepütz, C. M.; Cervellino, A.; Pauli, S. A.; Patterson, B. D.; Marchini, S.; Wintterlin, J.; Moritz, W.; Greber, T. *Phys. Rev. Lett.* **2008**, *101*, 126102.

(22) Moritz, W.; Wang, B.; Bocquet, M. L.; Brugger, T.; Greber, T.; Wintterlin, J.; Günther, S. *Phys. Rev. Lett.* **2010**, *104*, 136102.

(23) Thürmer, K.; Bartelt, N. C. *Phys. Rev. Lett.* **2008**, *100*, 186101.

(24) Lebedeva, I. V.; Knizhnik, A. A.; Popov, A. M.; Ershova, O. V.; Lozovik, Y. E.; Potapkin, B. V. *Phys. Rev. B* **2010**, *82*, 155460.

(25) Cui, Y.; Fu, Q.; Bao, X. *Phys. Chem. Chem. Phys.* **2010**, *12*, 5053−5057.

(26) Zhang, H.; Fu, Q.; Cui, Y.; Tan, D.; Bao, X. *J. Phys. Chem. C* **2009**, *113*, 8296−8301.

(27) Sutter, P.; Sadowski, J. T.; Sutter, E. A. *J. Am. Chem. Soc.* **2010**, *132*, 8175−8179.

(28) Xu, K.; Cao, P.; Heath, J. R. *Science* **2010**, *329*, 1188−1191.

(29) Cicero, G.; Grossman, J. C.; Schwegler, E.; Gygi, F.; Galli, G. *J. Am. Chem. Soc.* **2008**, *130*, 1871−1878.

(30) Feibelman, P. J. *Science* **2002**, *295*, 99−102.

(31) Corriol, C.; Calleja, F.; Arnau, A.; Hinarejos, J. J.; Vázquez de Parga, A. L.; Hofer, W. A.; Miranda, R. *Chem. Phys. Lett.* **2005**, *405*, 131−135.

(32) Xu, S. C.; Irle, S.; Musaev, D. G.; Lin, M. C. *J. Phys. Chem. C* **2007**, *111*, 1355−1365.

(33) Li, J. L.; Kudin, K. N.; McAllister, M. J.; Prud'homme, R. K.; Aksay, I. A.; Car, R. *Phys. Rev. Lett.* **2006**, *96*, 176101.

(34) Fujii, S.; Enoki, T. *J. Am. Chem. Soc.* **2010**, *132*, 10034−10041.

(35) Jiao, L.; Wang, X.; Diankov, G.; Wang, H.; Dai, H. *Nat. Nanotechnol.* **2010**, *5*, 321−325.

(36) Michaelides, A.; Alavi, A.; King, D. A. *J. Am. Chem. Soc.* **2003**, *125*, 2746−2755.

(37) Wehling, T. O.; Lichtenstein, A. I.; Katsnelson, M. I. *Appl. Phys. Lett.* **2008**, *93*, 202110.

(38) Nair, R. R.; Wu, H. A.; Jayaram, P. N.; Grigorieva, I. V.; Geim, A. K. *Science* **2012**, *335*, 442−444.

(39) Ajayan, P. M.; Yakobson, B. I. *Nature* **2006**, *441*, 818−819.

(40) Han, M. Y.; Ozyilmaz, B.; Zhang, Y. B.; Kim, P. *Phys. Rev. Lett.* **2007**, *98*, 206805.